Modeling the unstable DelftaCopter vertical take-off and landing tailsitter unmanned air vehicle in hover and forward flight from flight test data

De Wagter, Christophe; Meulenbeld, Joost

International Journal of Micro Air Vehicles

Modeling the unstable DelftaCopter vertical take-off and landing tailsitter unmanned air vehicle in hover and forward flight from flight test data

Christophe De Wagter and **Joost Meulenbeld**

Abstract

The DelftaCopter is a tilt-body tailsitter unmanned air vehicle which combines a large swashplate controlled helicopter rotor with a biplane delta-wing. Previous research has shown that the large moment of inertia of the wing and fuselage significantly interacts with the dynamics of the rotor. While this rigid rotor cylinder dynamics model has allowed initial flight testing, part of the dynamics remains unexplained. In particular, higher frequency dynamics and the forward flight dynamics were not modeled. In this work, the cylinder dynamics model is compared with the tip-path plane model, which includes the steady-state flapping dynamics of the blades. The model is then extended to include the wing and elevon dynamics during forward flight. Flight test data consisting of excitations with a large frequency content are used to identify the model parameters using grey-box modeling. Since the DelftaCopter is unstable, flight tests can only be performed while at least a rate feedback controller is active. To reduce the influence of this active controller on the identification of the dynamics, one axis is identified at a time while white noise is introduced on all other axes. The tip-path plane model is shown to be much more accurate in reproducing the high-frequency attitude dynamics of the DelftaCopter. The significant rotor–wing interaction is shown to differ greatly from what is seen in traditional helicopter models. Finally, an Linear-Quadratic Regulator (LQR) controller based on the tip-path plane model is derived and tested to validate its applicability. Modeling the attitude dynamics of the unstable DelftaCopter from flight test data has been shown to be possible even in the presence of the unavoidable baseline controller.

Introduction

Unmanned air vehicles (UAVs) have enabled new applications in many areas.[1] A wide range of those applications benefits from long endurance combined with vertical take-off and landing (VTOL) capability. Hybrid UAV combine the advantage of helicopter hovering and fixed-wing range efficiency.[2] One of the many concepts for combining long range with VTOL is the tailsitter or tilt-body hybrid UAV.[3] This concept has its rotors pointed upwards during hover, but can tilt downward by 90° to transition to forward flight. During forward flight, the wing provides the required lift, while the rotor only counters the drag.

Many tailsitter concepts have been proposed. Using at least four rotors in hover combined with traditional multicopter control is the earliest and most common solution. Examples include the QuadShot[4] and the VertiKUL.[5] A dynamic model for such a platform has been proposed by Smeur et al.[6]

Reducing the number of rotors, Bataillé et al.[7] have proposed two counter-rotating in-line propellers on their Vertigo platform. The counter-rotating small propellers reduce the gyroscopic effects of the propellers

Micro Air Vehicle Lab, Delft University of Technology, the Netherlands

Corresponding author:
Christophe De Wagter, Micro Air Vehicle Lab, Delft University of Technology, Kluyverweg 1, 2629HS Delft, the Netherlands.
Email: c.dewagter@tudelft.nl

on the body to levels where it does not need to be compensated for by the attitude controller. Similarly, when both propellers are in-plane but side by side, the gyroscopic effect of both counter-rotating propellers cancel each other out pretty well. This was for instance shown in the control of the MAVION by Lustosa et al.[8] and the Cyclone by Bronz et al.[9] Wong et al.[10] have proposed a similar concept but with variable pitch propellers, and show that a controller based on a simple second-order model achieves acceptable control. But for all three, the biggest difficulty was coping with the highly non-linear and imprecisely modeled effectiveness of the aerodynamic control surfaces.

To further increase hovering efficiency and control moments, De Wagter et al.[11] have proposed the DelftaCopter tailsitter (see Figure 1) which has a single rotor with cyclic and collective blade pitch control. The rotor inertia of the DelftaCopter was shown to be sufficiently large to significantly affect the dynamics of the rigid body, yet is too small to act as a pure gyroscope as in a conventional helicopter described by Kondak et al.[12] The proposed model allowed to create a working controller, but only modeled the low-frequency dynamics in hover.[13] Several other single rotor concepts were proposed like the AeroVel Flexrotor,[14] but these do not report the same properties as the DelftaCopter.

While black-box modeling has recently shown practical results in modeling unconventional UAV,[16] this work will extend a model of a tailsitter UAV with a single large rotor to better model high-frequency responses and forward flight and will use grey-box parameter estimation.

The section "Single Rotor Tailsitter Modeling" first compares the different models that can be applied to single rotor tailsitters, and the section "State-Space Description" formulates the state-space model.

Figure 1. The DelftaCopter tailsitter UAV in hovering flight. DelftaCopter has a single large rotor with collective and cyclic blade pitch control, two small torque countering tip propellers and a pair of delta-wings placed in biplane configuration. The tips form the landing legs and provide yaw stability in forward flight. It weighs 4.3 kg and was designed to fly 60 km in the Outback Medical Challenge 2016.[15]

The section "System Identification" describes how system identification is performed in-flight on an unstable platform. The section "Identification Results in Hover" describes the results of the system identification. With the fitted models, a controller was designed and implemented for hover in the section "Model Verification through Controller Derivation". The model is extended to model the forward flight dynamics in the section "Forward Flight Modeling". Finally, the conclusions are presented.

Single rotor tailsitter modeling

Modeling helicopter rotor dynamics can be categorized into roughly three levels of simplification in blade flapping dynamics.

Flapping dynamics

The first and most elaborate approach is to deal with the blade flapping explicitly and to include the flapping angle of every individual blade as a state of the model. This requires many physical parameters to be accurately identified.

Bramwell et al.[17] proposed such a model where θ is the blade pitch angle, Ψ is the in-plane rotation of the blade from the back of the helicopter and θ_0 is the collective pitch angle. δ_x and δ_y are the cyclic pitch settings and influence the blade pitch through the swashplate as follows

$$\theta = \theta_0 - \delta_x \cos\Psi - \delta_y \sin\Psi \qquad (1)$$

This variation of pitch angle θ over the rotation Ψ from equation (1) will generate differences in aerodynamic forces which, combined with aerodynamics and inertial forces, in turn make the blades flap up and down.

Tip-path-plane

A first simplification is to relate the attitude dynamics of the helicopter to the tip-path plane (TPP). This is the plane in which the tips of the rotor travel and is shown in Figure 2. Mettler[18] has derived a TPP model by neglecting high-frequency dynamics of the rotor. The TPP is represented by the longitudinal and lateral angles a and b in radians between the TPP and a plane perpendicular to the rotor axis. These correspond to the steady-state flapping angles when the blade is aligned with the X and Y axis. The TPP angles change under influence of control inputs, rotations of the fuselage and gyroscopic precession of the rotor. The fuselage is a separate rigid body and a moment is transferred from the rotor to the fuselage if the a and b
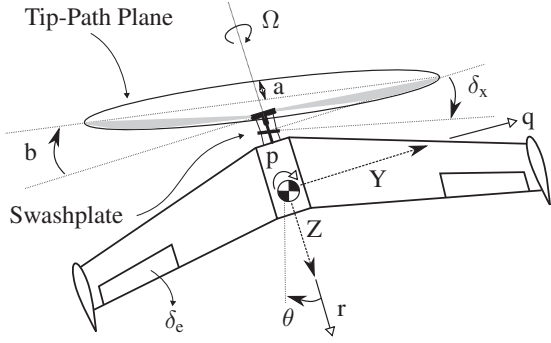
Figure 2. Helicopter tip-path plane (TPP) model showing the tip angles a and b, the cyclic deflections δ_x and δ_y as well as the body X, Y and Z axes and p, q and r turn rates. Ω is the rotor speed.

angles are non-zero, due to the effective spring between the rotor blade and axis and the offset of thrust application point on the rotor and the center of mass of the fuselage.[18,19]

Cylinder dynamics model

A final simplification is to ignore the flapping dynamics completely and treat the rotor as a rigid disc or cylinder. This model is widely used for small helicopters.[20–22] A TPP model can be transformed into a model without flapping dynamics by setting the derivatives of the a and b angles to zero. This simplification can be valid if the inertia proportion of the fuselage compared to the rotor is very small or the hinge spring forces are very large.[19] The model without flapping dynamics is referred to as a cylinder dynamics (CD) model.

State-space description

The TPP and CD models will be given as linear time-invariant models in state-space form

$$\dot{\bar{x}} = A\bar{x} + B\bar{u} \tag{2}$$

$$\bar{y} = C\bar{x} + D\bar{u} \tag{3}$$

TPP model

The TPP model has been adapted from Mettler.[18] Only the attitude dynamics are considered and the Hiller bar dynamics are removed. The state vector becomes $\bar{x} = (p, q, a, b)^T$ with p and q being the roll and pitch rates expressed in radians per second. The input vector is $\bar{u} = (\delta_x, \delta_y)^T$ where δ_x and δ_y are measured in percent. The observable states are $\bar{y} = (p, q)$. The state-space A and B and C matrices for the TPP model are given in

equations (4) to (6). The C-matrix shows that only the body rates are measurable and the D-matrix consists of only zeros. The model has nine parameters that need to be identified: L_b and M_a represent the spring constants of the TPP and consist of the combined stiffness of the blade and blade hinge and the offset between the rotor thrust vector and center of mass of the fuselage. τ_{f_n} is the time constant of the TPP dynamics. A_{b_n} and B_{a_n} are cross-coupling terms that describe how the TPP interchanges the a and b angles over time. The four parameters in the B-matrix give the actuator effectiveness. The dependence of several parameters on the rotor r/min Ω is showing in $\tau_f = \tau_{f_n}/\Omega$, $A_b = A_{b_n}/\Omega^2$ and $B_a = B_{a_n}/\Omega^2$ (Mettler,[18] sec. 2.3). This results in

$$A_{\text{TPP}} = \begin{bmatrix} 0 & 0 & 0 & L_b \\ 0 & 0 & M_a & 0 \\ 0 & -1 & -\dfrac{\Omega}{\tau_{f_n}} & \dfrac{A_{b_n}}{\Omega\,\tau_{f_n}} \\ -1 & 0 & \dfrac{B_{a_n}}{\Omega\,\tau_{f_n}} & -\dfrac{\Omega}{\tau_{f_n}} \end{bmatrix} \tag{4}$$

$$B_{\text{TPP}} = \begin{bmatrix} 0 & 0 \\ 0 & 0 \\ \dfrac{A_{lat}\,\Omega}{\tau_{f_n}} & \dfrac{A_{lon}\,\Omega}{\tau_{f_n}} \\ \dfrac{B_{lat}\,\Omega}{\tau_{f_n}} & \dfrac{B_{lon}\,\Omega}{\tau_{f_n}} \end{bmatrix} \tag{5}$$

$$C_{\text{TPP}} = \begin{bmatrix} 1 & 0 & 0 & 0 \\ 0 & 1 & 0 & 0 \end{bmatrix} \tag{6}$$

CD model

The CD model state variables are only the body rates $\bar{x} = (p, q)^T$, and the input is the same as for the TPP model. Both the A- and B-matrices consist of four identifiable parameters, as shown in equations (7) and (8) below. All elements in A can be related to the steady-state solution of the a and b states in the TPP model, or through gyroscopic moments and aerodynamic damping.

$$A_{cyl} = \begin{bmatrix} L_p & L_q \\ M_p & M_q \end{bmatrix} \tag{7}$$

$$B_{cyl} = \begin{bmatrix} L_{lat} & L_{lon} \\ M_{lat} & M_{lon} \end{bmatrix} \tag{8}$$

Relation between CD and TPP

In Mettler's model, only the a and b states drive the angular accelerations in q and p states, respectively. This means that instead of determining the body angular acceleration directly using the control input as in the CD model, control inputs first affect the dynamics of the TPP, which, in turn, influences the body angular acceleration.

The steady-state solution resulting from $\dot{a} = \dot{b} = 0$ in the TPP models allows substitution of steady-state a and b values in the $\dot{p}$ and $\dot{q}$ equations, which then yields a comparable system as the CD model, with every CD model parameter linked directly to a combination of parameters in the TPP model.[19]

System identification

Unstable platform

To identify the parameters from the derived models, a grey-box parameter estimation procedure is used based on the input–output response found in flight test data. To get the best identification results, the system should be measured open-loop. In the case of the DelftaCopter, this is not possible because it has an unstable attitude and requires at least a rate controller to fly. Constraining the motion to one axis at a time is not an option as the rotor dynamics create couplings between pitch and roll that would then not be identified. Initial attempts by hanging the DelftaCopter using a rope introduced too many external forces on the system and made identification impossible. Therefore, system identification was finally performed in free flight using a simple linear P feedback controller on rate. The controller used during system identification is a simplified version of the one described by De Wagter and Smeur[13] in which the rate coupling compensations are removed

$$\begin{bmatrix} \delta_x \\ \delta_y \end{bmatrix} = G^{-1} \begin{bmatrix} K_p p_{err} \\ K_q q_{err} \end{bmatrix} \tag{9}$$

where K_p and K_q are proportional gains, p_{err} and q_{err} are the rate errors and 2 by 2 matrix G^{-1} is the inverted control effectiveness.

Noise

To lower the risk of false correlation between different inputs and states that become coupled through the attitude controller, Tischler and Remple[23] suggested adding white noise to every axis independently. This reduces the chance of false correlations and hereby

allows in-flight system identification of an unstable platform if a simple baseline controller is available.

Finally, further complicating system identification, not all states can be measured in-flight. As represented in the C-matrix in equation (6), only the body rates can be measured and the a and b states are not directly observable. Absolute values of a and b are thereby not validated.

Flight maneuvers

Flight tests were performed in an indoor environment without wind or turbulence. As proposed by Tischler and Remple,[23] a "chirp-shaped" actuator deflection is applied on each control input separately. A chirp is a sine wave with a frequency increasing continuously over time.

The white noise that is also injected on all axes during the chirp is filtered with a first-order low-pass filter with the cut-off at the highest frequency of the chirp. An exponential-time chirp is used to have enough content at the lower frequencies.

The chirp signal is generated and added to the controller signal and the resulting actuator signal is stored with the gyroscope measurements on an SD-card at a frequency of 512 Hz using a custom Paparazzi-UAV autopilot.[24]

The exponential-time chirp formulation by Tischler and Remple[23] was implemented as[a]

$$K = C_2 \left(e^{\left(C_1 \cdot \frac{t}{\Delta_t} \right)} - 1 \right) \tag{10}$$

$$\phi = 2\pi \left(f_0 \cdot t + (f_1 - f_0) \cdot \left(\frac{\Delta_t}{C_1} \cdot K - C_2 \cdot t \right) \right) \tag{11}$$

where C_1 and C_2 are coefficients, t is the time, Δ_t is the chirp duration in seconds, f_0 and f_1 are the start and stop frequencies, ϕ is the phase of the chirp and the amplitude of the chirp in function of time is $s(t) = \sin(\phi)$. The lower frequency and amplitude are limited by the maximal roll angle that the system is allowed to reach during the test. The maximal attitude angles were not permitted to grow larger than about 30°. The chirp settings are given in Table 1. The noise fraction is the ratio between the amplitude of the chirp and the standard deviation of the white noise that is filtered and added to the chirp signal. From video it was found that the two main eigenfrequencies of the DelftaCopter lie well within the range of the chirp. Tests at much higher command frequencies confirmed that there is almost no body rate anymore besides higher vibration at the rotor frequency.

Post-processing

To cope with low-quality sensor data, some post-processing was performed as in Dorobantu et al.[25] The onboard flight test data were filtered digitally using an ideal low-pass filter with a cut-off frequency of 15 Hz. This removes vibrations caused by the DelftaCopter rotor which rotates at about 27.5 Hz. The inputs were centered around zero to remove any input bias. The resulting time domain chirp logfiles were used to fit the parameters using the MATLAB[b] system identification toolbox greyest function.

Identification results in hover

The full-time sequences including fitted models for a roll chirp are shown in Figure 3. The figure shows the measured pitch and roll rates together with the predicted pitch and roll rates from both CD and TPP models. The predicted pitch and roll rates are obtained by feeding the logged inputs into the respective models. The non-zero pitch rate q is a result of the pitch–roll coupling introduced by the rotor. It is clear that the CD model can accurately predict the response up to a certain frequency, but does not include the eigenfrequency which is excited at around 28.5 s. The TPP dynamics model has four states and was found to have two pairs of complex poles which leads to two eigenfrequencies. The slowest eigenfrequency is the same as in the CD model, while the highest eigenfrequency corresponds to the faster oscillations seen in the chirp plots. A pitch chirp is shown in Figure 4. In this chirp, the mismatch between the CD model and measurements is even worse.

Validation maneuvers

To validate the identified model parameters, pitch and roll doublets were recorded separately and not used in the identification. Figure 5 shows pitch and roll commands manually given by a pilot, which represent normal flight maneuvers of the DelftaCopter. While the roll rate is relatively well captured by both models, even at these relatively low-frequency doublets, the pitch rate is significantly off in the case of the CD model.

Table 2 shows the eigenfrequencies of both identified TPP and CD state-space systems. The first pole-pair has almost the same eigenfrequency in both models,

Table 1. Exponential-time chirp settings.

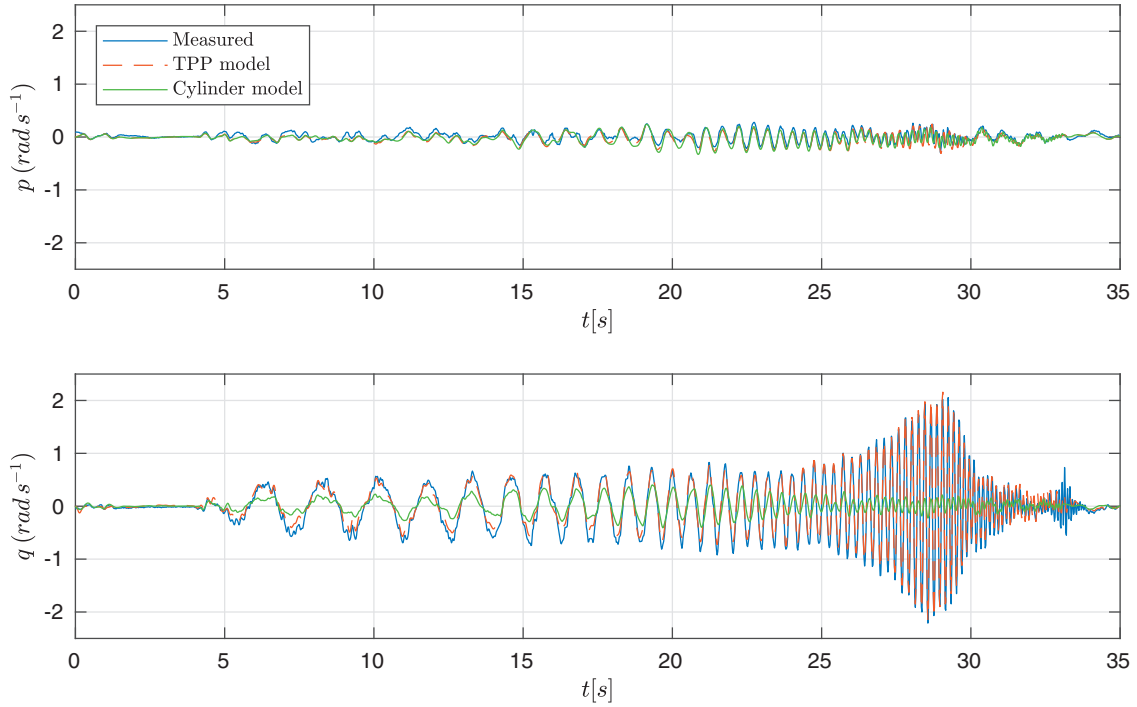| Variable	Value
Start frequency f_0	0.5 Hz
End frequency f_1	10 Hz
Noise fraction	0.2
C_1	4
C_2	$\frac{1}{e^{C_1}-1}$
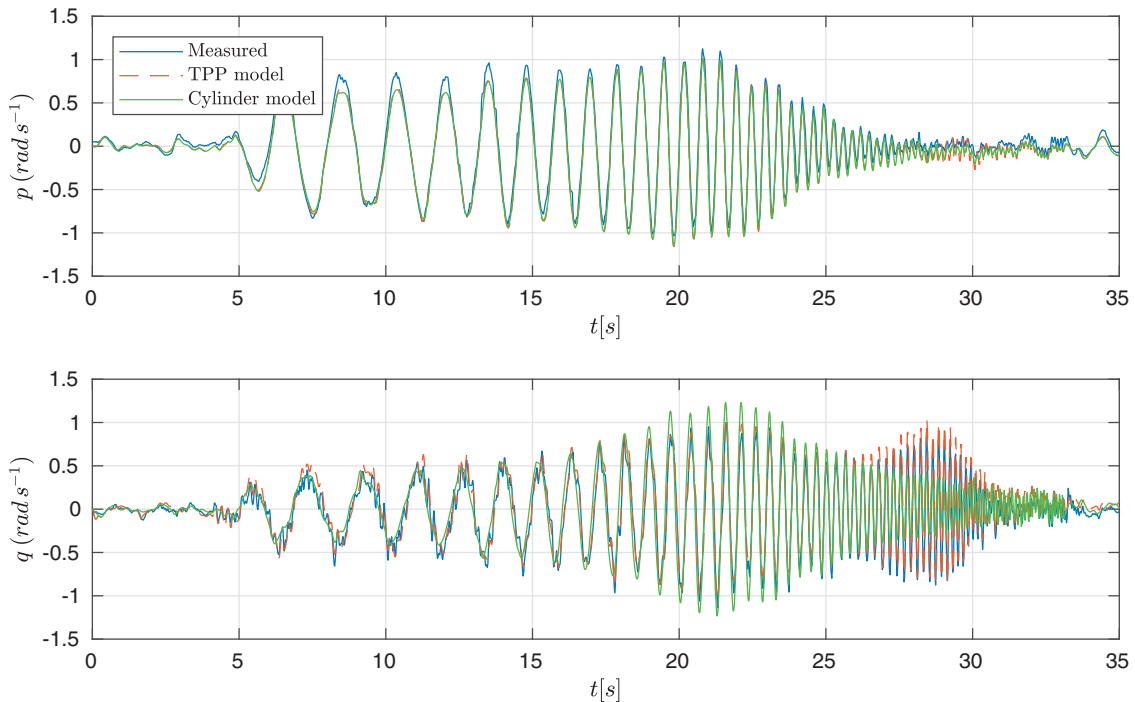
Figure 3. Chirp on the roll axis in hover. The very significant pitch response to the roll chirp is mainly due to pitch–roll couplings. The TPP model is much better at reproducing the measured pitch signals in the higher frequency range.

Figure 4. Chirp on the pitch axis in hover. The roll motion due to pitching is not severe due to the high roll inertia compared to the pitch inertia. The CD model accuracy at low frequencies is clearly worse than the TPP model.
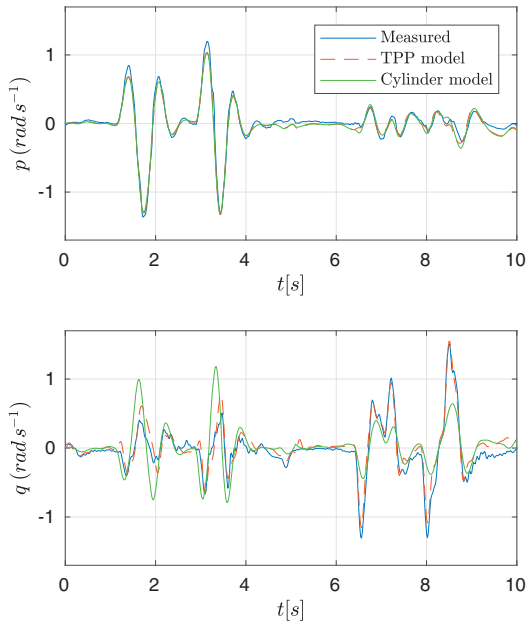
Figure 5. Validation flight test sequence flown in manual control consisting of first a roll doublet and then a pitch doublet. The roll response is quite accurately modeled by both models, while the pitch response is clearly better in the TPP model.

Table 2. Comparison of eigenfrequencies of the TPP and CD models.

Pole	Frequency (Hz)	Damping (–)
CD model		
1–2	1.54	0.35
TPP model		
1–2	1.64	0.39
3–4	5.04	0.22

CD: cylinder dynamics; TPP: tip-path plane.

dynamics are completely damped out, as is most obvious in Figure 4.

Results

Table 3 lists all the identified model parameters. These are the matrix elements in equations (4), (5), (7) and (8) where the following substitutions were performed

$$\tau_f = \tau_{f_n}/\Omega \tag{12}$$

$$A_b = A_{b_n}/\Omega^2 \tag{13}$$

$$B_a = B_{a_n}/\Omega^2 \tag{14}$$

which means that at lower frequencies both models respond comparably. However, the higher eigenfrequency of the flapping dynamics model is not present in the CD model, which explains why high-frequency

The difference in roll and pitch inertia of the DelftaCopter is apparent from the L_b and M_a values, which differ by a factor of 4.8.

Fitting quality

To assess the fitting quality, the coefficient of multiple correlation (CoMC) is used as given in equation (15), where 100% constitutes a perfect match

$$R = \left(1 - \frac{\|s - \hat{s}\|}{\|s - \bar{s}\|}\right) \quad (15)$$

in which R is the CoMC, s is the measured signal, $\hat{s}$ is the model output and $\bar{s}$ is the average of the measured signal. The CoMC of both identified models on the identification and validation data is given in Table 4. For both the chirp and validation doublets, the CoMC of the roll response of both models is very similar. Interestingly, the CoMC of the pitch on the validation doublet is lower than on the chirp data. This shows that even the TPP does not capture all the dynamics or the optimizer might overfit the chirp data. When looking back at Figure 5, the time series of q shows that the biggest error in pitch seems to occur when large roll rates occur. This points to uncaptured couplings, which could, for instance, come from hinge spring non-linearities.

Table 3. The identified TPP and CD model parameters.

TPP	Value	CD	Value
A_b	−1.338	L_p	−2.056
B_a	1.448	M_p	10.536
L_b	147.548	L_q	−7.900
M_a	713.378	M_q	−4.777
τ_f	0.091	L_{lat}	−5.361
A_{lat}	−0.282	M_{lat}	−67.573
A_{lon}	0.296	L_{lon}	9.917
B_{lat}	0.524	M_{lon}	11.136
B_{lon}	−0.050		

CD: cylinder dynamics; TPP: tip-path plane.

Table 4. CoMC of the TPP and CD model fits on identification chirps and validation doublets.

Axis	TPP model	CD model
Chirp		
p	77.8%	77.2%
q	77.3%	25.9%
Doublets		
p	77.6%	76.7%
q	64.7 %	20.0%

CD: cylinder dynamics; TPP: tip-path plane.

Reproducibility

To validate that the parameters were not overfitted to a particular chirp, the TPP model was fitted to two different sets of chirp data and their fitted parameters were compared. The highest single change in model parameter between the two sets of chirps was 7.7%, but the eigenfrequencies and damping ratios of the systems differed not more than 0.9% and 1.8%, respectively.

RPM dependence of parameters

The model from Mettler et al.[19] which is simplified in equations (4), (5), (7) and (8) contains the rotor r/min Ω and is expected to compensate changes in rotor speed. To assess if the remaining model parameters remain constant at different rotor rotational speeds, a range of r/min between 1500 and 1650 was tested.

Although the rotor r/min was varied only 10%, some model parameters, which should stay constant, showed changes of up to 185% (B_{lon}) with many others changing tens of percents as shown in Table 5. The meaning of these changes in model parameters in terms of model response is analyzed by comparing the eigenfrequency and damping of the model fitted on the 1650 r/min data with the model fitted on 1500 r/min and then corrected to 1650 r/min using equations (12) to (14). The largest change in eigenfrequency was only 4%, while the largest change in damping ratio was up to 28%. This leads to the conclusion that mainly the damping properties still contain unmodeled dynamics. The CoMC of this model fitted on 1500 r/min was 72.4% in roll and 67.1% in pitch when tested on the same 1650 r/min chirp as in Table 4. Further research is thus needed to obtain models that generalize well with different rotor r/mins.

Model verification through controller derivation

To test the applicability of the model, it was used to derive a linear rate controller which was subsequently

Table 5. The identified TPP parameters in function of r/min.

r/min	1499.8	1549.8	1599.7	1649.6
A_{b_n}	−45350	−55960	−54590	−57000
B_{a_n}	46180	49720	57790	62700
L_b	176.100	179.400	178.100	181.200
M_a	746.800	754.000	754.200	760.900
τ_{f_n}	14.010	15.980	18.370	19.350
A_{lat}	−0.157	−0.173	−0.243	−0.268
A_{lon}	0.240	0.270	0.291	0.302
B_{lat}	0.484	0.494	0.564	0.599
B_{lon}	−0.040	−0.063	−0.098	−0.114

tested. Since the TPP angles a and b are not measured onboard the DelftaCopter, a linear observer was created in the form

$$\dot{\hat{x}} = A\hat{x} + B\bar{u} + L(\bar{y}_{measured} - \hat{y}) \qquad (16)$$

$$\hat{y} = C\hat{x} + D\bar{u} \qquad (17)$$

in which $\hat{x}$ is the current state estimate and L is the correction matrix. The A, B and C matrices are as given in equations (4) to (6) and the parameters are shown in Table 3.

The L matrix is chosen using pole placement, setting the poles of the observer at $(-50, -50, -51, -51)$. This is small enough to add some damping to the vibrations caused by the rotor on the gyroscope readings.

The controller is designed using the feedback law

$$\bar{u} = -K\hat{x} + g\bar{y}_{ref} \qquad (18)$$

in which $\bar{y}_{ref}$ is the reference attitude rate and the steady-state gain of the controlled system is g, with

$$g = (C(-A + BK)^{-1})^{-1} \qquad (19)$$

The gain matrix K is selected using LQR. This finds the optimal gain matrix K for the system minimizing a cost function of state and inputs. The cost matrices of the LQR design for the states p and q is set to 1. Since the actual value of the a and b states do not matter, they were given a cost of only 0.001.

Several controllers were then designed with different costs on system input deflections. The lower the cost on the input, the larger the allowed deflections and the faster the controller steers the system. The input cost of 5 made the system the fastest without introducing oscillations.

The controlled system response is shown in Figure 6. It can be seen that the roll response has a small delay, but the roll measurement follows the command well. The pitch response shows a coupling when larger roll rates are present. The pitch response is also larger in magnitude than the commanded rate.

The fact that the model can be used to design a controller for the DelftaCopter further confirms that the TPP model covers the most essential dynamics of the platform. On the other hand, it confirms the findings in Table 4 that not all DelftaCopter dynamics are captured in this simplified model.

Forward flight modeling

In forward flight, the DelftaCopter pitches down 90° such that the wings are almost level with the ground, as shown in Figure 7. The airspeed increases and the
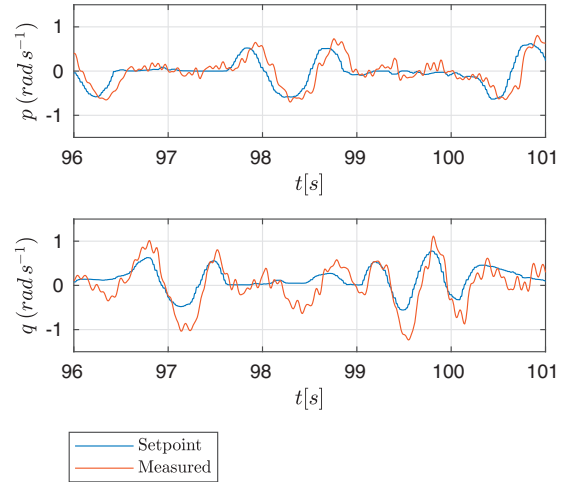
Figure 6. Performance test of an LQR controller derived directly from the identified TTP DelftaCopter model. The pilot manually commands the attitude rate of the DelftaCopter. The roll response has a small delay with respect to the command but otherwise has adequate tracking performance. The pitch rate shows coupling with the roll and the response shows larger values than the command.
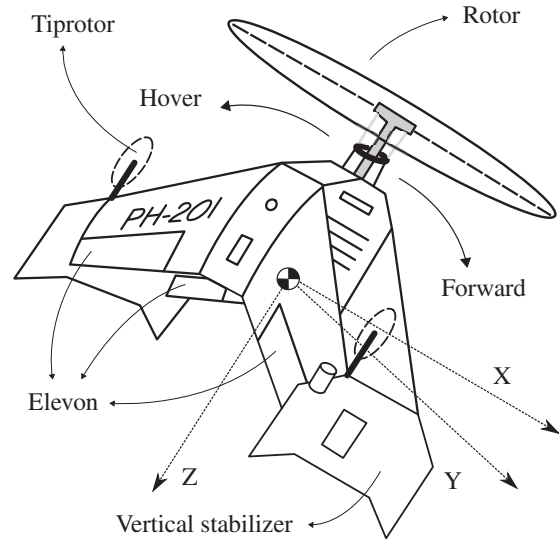
Figure 7. The DelftaCopter tailsitter UAV has a single main rotor which points up and provides lift during hover. Two tip props provide counter torque in hover, and the swashplate gives lateral and vertical control. In forward flight, the entire vehicle tilts 90° down and the rotor provides thurst while the biplane delta-wings provide lift, and the elevons provide most of the control. In forward flight de tip propellers are disabled.

wings generate the required lift to maintain altitude, while the main rotor is now providing forward pointed thrust.

In fast forward flight, the aerodynamic surfaces play a significant role in the balance of moments of the

DelftaCopter attitude dynamics. The TPP and CD hover models are therefore extended. To keep a linear model, linear aerodynamic moments are assumed.

Aerodynamic surface models

The DelftaCopter has four movable surfaces that together perform the role of aileron and elevator of the delta-wing. The ailerons apply a moment on the body along the Z axis, which is the axis of rotation of the rotor and points forward during forward flight. Since the yaw angle is not included in the model and differential aileron drag of the ailerons is further neglected, it is not added to the model. The elevator can generate a significant moment in the pitch axis and is included in the model as parameter M_{elev}. The longitudinal damping moment of the wings due to a pitch-rate q is named M_q and lateral damping due to rate p is called L_p. Note that for the DelftaCopter, the body X axis point down and represents the yawing of the delta-wing. In the CD model, these extra effects are lumped into the parameters already present, while in the TPP model these damping parameters need to be added. The state vector x is the same as the model in hover, while the input vector is extended to $\bar{u} = (\delta_x, \delta_y, \delta_e)^T$, with δ_e being the elevator deflection.

The resulting TPP state-space system for forward flight thereby becomes

$$A_{\text{TPP,FW}} = \begin{bmatrix} L_p & 0 & 0 & L_b \\ 0 & M_q & M_a & 0 \\ 0 & -1 & -\dfrac{\Omega}{\tau_{f_n}} & \dfrac{A_{b_n}}{\Omega \tau_{f_n}} \\ -1 & 0 & \dfrac{B_{a_n}}{\Omega \tau_{f_n}} & -\dfrac{\Omega}{\tau_{f_n}} \end{bmatrix} \quad (20)$$

$$B_{\text{TPP,FW}} = \begin{bmatrix} 0 & 0 & 0 \\ 0 & 0 & M_{elev} \\ \dfrac{A_{lat}\,\Omega}{\tau_{f_n}} & \dfrac{A_{lon}\,\Omega}{\tau_{f_n}} & 0 \\ \dfrac{B_{lat}\,\Omega}{\tau_{f_n}} & \dfrac{B_{lon}\,\Omega}{\tau_{f_n}} & 0 \end{bmatrix} \quad (21)$$

L_p and M_q represent aerodynamic damping on the roll and pitch rate. As before, the parameters L_b and M_a of the TPP model are the representative spring constants, and their physical meaning is given by Mettler,[18] sec. 3.1. M_a is defined as

$$M_a = \frac{k_\beta + hT}{I_{yy}} \quad (22)$$

This relates the TPP angle a to the angular acceleration $\dot{q}$ of the body and contains a rotor stiffness term k_β and moment due to the offset h of where the thrust T acts on the body compared to the center of gravity. De Wagter and Smeur[13] estimated the rotor blade spring stiffness k_β to be $\approx 88\,\text{N m rad}^{-1}$. The contribution to the moment caused by the thrust at maximum weight $hT \approx hmg \approx 0.15 \cdot 4.5 \cdot 9.81 = 6.6\,\text{N m rad}^{-1}$. In forward flight, the actual thrust will be much smaller than the full weight. Therefore, the contribution of the variable thrust on the parameters L_b and M_a is assumed to be very small and the parameters are further assumed to be constant.

The $A_{cyl,FW}$ matrix in the CD model in forward flight is the same as in hover given in equation (7), and the damping moments from the rotor and wing are mixed. The $B_{cyl,FW}$ matrix is as given in equation (8) with the addition of the third input δ_e which after linearization is modeled to yield a pitch acceleration $\dot{q}$ through parameter M_{elev}.

Results

The parameters are fitted from measurements obtained during chirp maneuvers on all three actuators $\bar{u}$ in steady level flight. The model fitting was always done using a different set of chirps than the validation chirps depicted in this work. Due to perturbations from amongst others the chirp itself, the airspeed fluctuates between $17\,\text{m s}^{-1}$ and $19.5\,\text{m s}^{-1}$, while the r/min fluctuates between 1550 and 1720. This r/min range is quite broad compared to the hover experiments, especially considering the observed sensitivity of parameters to the r/min.

The parameters of the TPP and CD models are given in Table 6. Comparing these with the hover parameters in Table 3 shows that both have comparable parameters for the rotor dynamics in the TPP

Table 6. The fitted values for the TPP and CD models in forward flight.

| TPP	Value	CD	Value
A_b	−0.908	L_p	−10.690
B_a	0.999	M_p	14.899
L_b	147.550	L_q	−9.251
M_a	713.380	M_q	1.050
τ_f	0.075	L_{lat}	6.605
A_{lat}	−0.196	M_{lat}	−70.459
A_{lon}	0.214	L_{lon}	−2.903
B_{lat}	0.440	M_{lon}	11.532
B_{lon}	−0.026	M_{elev}	10.263
L_p	−0.930		
M_q	4.691		
M_{elev}	37.752		

CD: cylinder dynamics; TPP: tip-path plane.
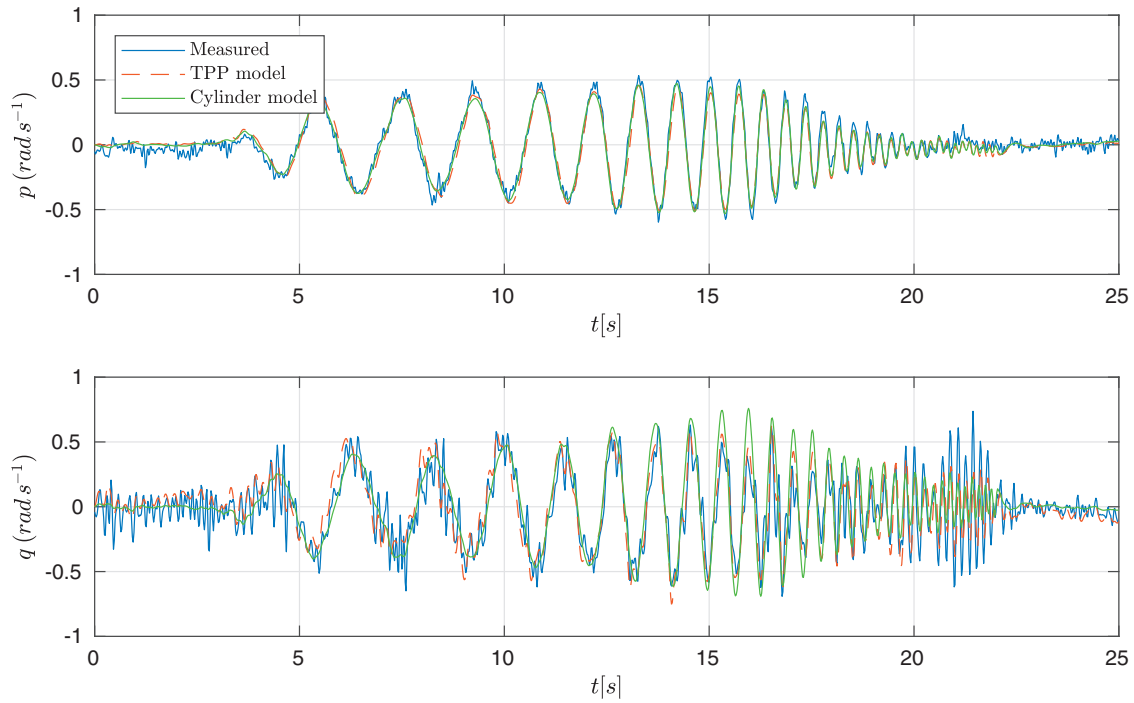
Figure 8. Validation chirp on the roll axis in forward flight. The pitch motions are mainly due to pitch-roll coupling. The TPP and CD model have a similar response. The high-frequency fluctuations in the pitch are due to the attitude controller which is active during the chirp.
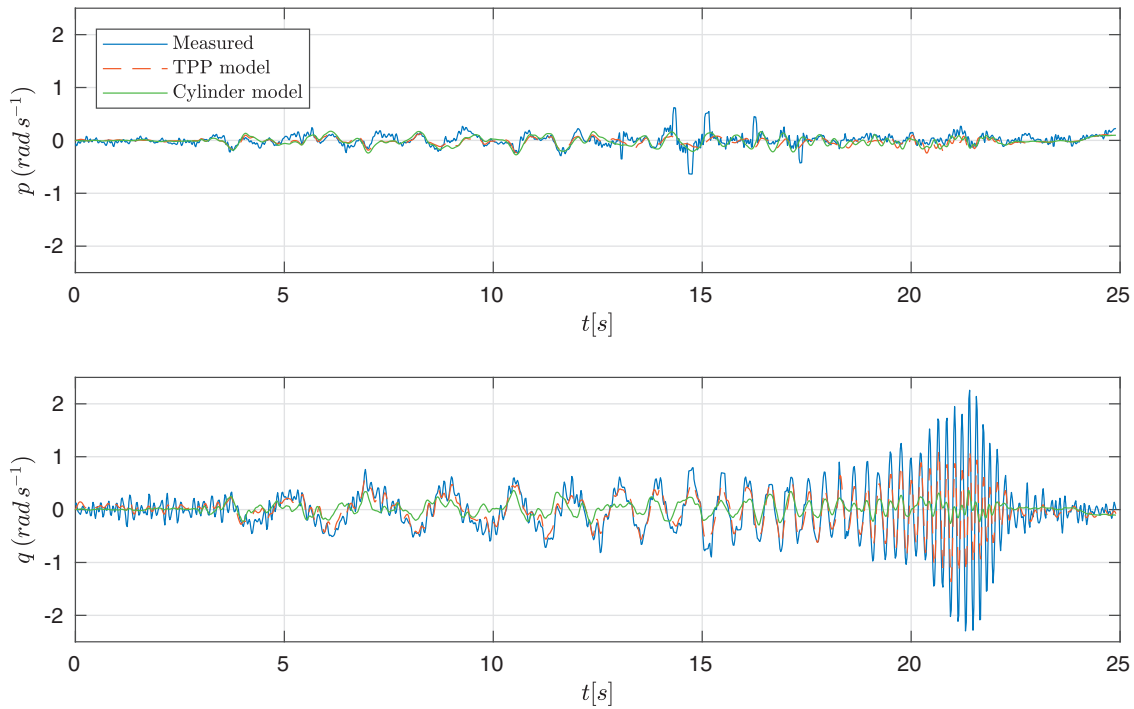
Figure 9. Validation chirp on the pitch axis in forward flight. The CD model accuracy is much worse than the TPP model, while the latter is also unable to follow the measurements at higher frequencies.
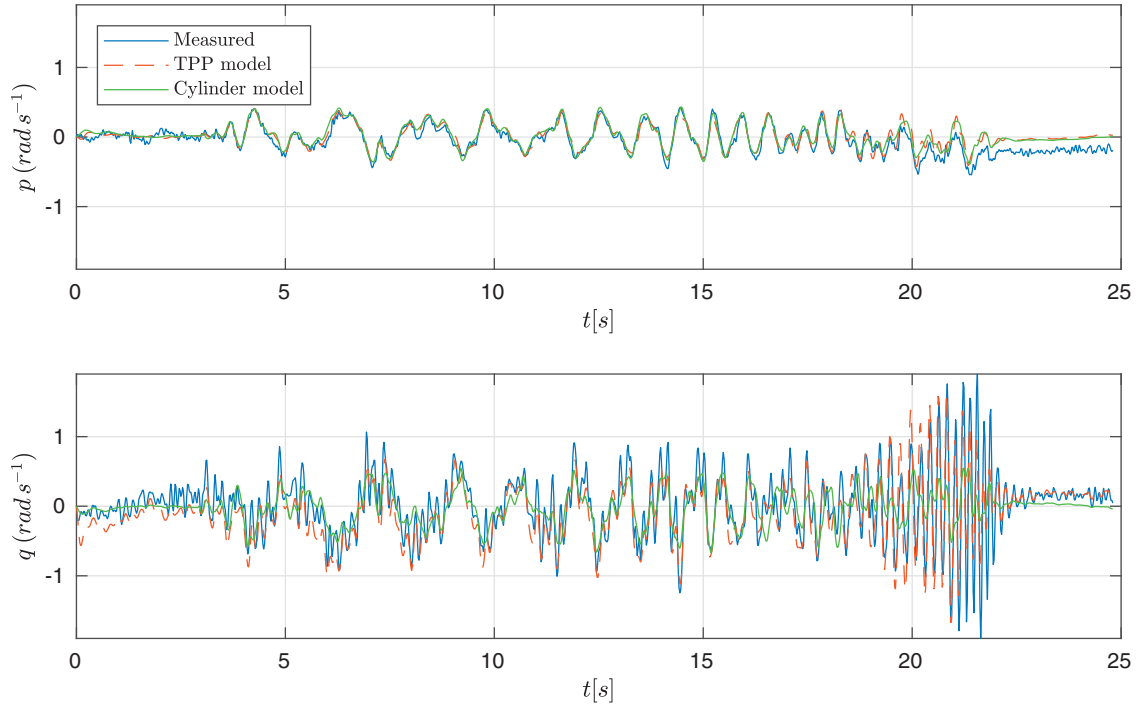
Figure 10. Validation chirp on the elevator axis in forward flight. The roll response p (yaw in fixed wing aircraft reference frame) is fitted accurately by both TPP and CD models, while in the pitch reponse q, the TPP models starts to show significant difference around 20 s as the CD model is unable to replicate those frequencies at all.

model. That the roll rate damping is very small is to be expected since the vertical stabilizing tips of DelftaCopter have a small moment arm to the center of mass.

Figures 8 to 10 show the measurements and the model responses of chirps on roll, pitch and elevator, respectively. The resulting TPP and CD model fits are overlayed in the figures and clearly show which frequencies are not well modeled.

It is clear that the TPP model is better at predicting the high-frequency response than the CD model, but the fit is not as good as for the hover model. This can be due to the r/min fluctuations or the TPP model. Another cause of model inaccuracy could be aerodynamic effects missing in the model or the energy exchange during the chirps. Atmospheric conditions are also less steady during outdoor forward flights than during the indoor hover tests. The angle of attack is not part of the model either and was not measured, but could have an important influence. Surprisingly, the M_q parameter is positive, implying a positive feedback loop on the pitch rate. This could be due to the missing of other influences in the model. The CoMC of the fits can be found in Table 7. Both fitting and validation percentages concern three chirps, one roll, one pitch and one elevator. The validation chirps and model responses can be found in Figures 8 to 10.

Table 7. Comparison of CoMC percentage as given in equation (15) for forward flight.

Axis	TPP model	CD model
Fitting		
p	66.0%	70.8%
q	54.7%	21.7%
Validation		
p	49.7%	53.1%
q	47.1%	17.0%

CD: cylinder dynamics; TPP: tip-path plane.

Conclusion

The DelftaCopter is a tailsitter UAV consisting of a single rotor with cyclic and collective pitch control on top of a delta-wing biplane. Previous research developed a CD model which assumes a rigid rotor.[13] This work compared the CD model with a linearized TPP model of the attitude dynamics based on work by Mettler.[18] A system identification modeling approach was chosen and chirps were used as system identification maneuver to fit a wide frequency range. The TPP model is shown to be much better at modeling the high-frequency response than the CD model. This is validated using manually flown doublets, for which the TPP response also shows better accuracy. In particular, the flapping dynamics modeled as the TPP significantly

influence the pitch dynamics of the DelftaCopter at about 5 Hz. It was shown that this model can be used for controller design by deriving an LQR attitude rate controller.

The relationship between the identified parameters and rotor r/min was found to be different than predicted from theory. This may be due to the lumping together of unmodeled effects into the present parameters, but is likely to be due to non-linear effects that the current state-space model has linearized. In particular, the rotor hinge spring is believed to have very non-linear characteristics.

For forward flight, the TPP and CD models were extended to include roll rate and pitch rate damping and to include a constant for the elevator effectiveness.

Some very particular characteristics of the DelftaCopter were also confirmed:

- The principal components for the actuation of pitch and roll are significantly different than in traditional helicopters and are not even perpendicular.
- The roll actuator mainly drives roll at low frequencies and mainly drives pitch at high frequencies.

Overall, the derived linear state-space model captures most of the dynamics of the DelftaCopter in the frequency range up to 10 Hz. Nevertheless, the data clearly shows that not all dynamics are modeled and more states and non-linearities have to be included to improve the modeling.

Recommendations

Due to technical constraints, the *a* and *b* angles of the TPP could not be measured. They were estimated using the derived model, but could not be validated. The angle of attack α or sideslip angle β of the delta-wing in forward flight could also not be measured, but could better model errors like the end of Figure 10 where sideslip or increased angle of attack could be the cause of the steady-state error.

Although separate tests have shown that the used *MKV HV9767* servos could track the required chirp commands with small deflections up to frequencies of over 20 Hz, the role of servo dynamics on the faster dynamics should be further investigated.

The dependency of model parameters on r/min needs further investigation as the expected theoretical relation could not be confirmed.

Finally, in forward flight, it is recommended to generalize the flight model for different airspeeds and r/min, as these values do change during normal flight conditions.

ORCID iD

Christophe De Wagter (iD) https://orcid.org/0000-0002-6795-8454

Notes

a. The chirp code is published open source at http://www.github.com/paparazzi/paparazzi as the sys_id_chirp module
b. Using MATLAB 2018a.

References

1. Valavanis KK. *Advances in unmanned aerial vehicles: state of the art and the road to autonomy*. Berlin: Springer, 2012.
2. Saeed AS, Younes AB, Cai C, et al. A survey of hybrid unmanned aerial vehicles. *Prog Aerosp Sci* 2018; 98: 91–105.
3. Herbst S, Wortmann G and Hornung M. Conceptual design studies of vertical takeoff and landing remotely piloted aircraft systems for hybrid missions. *CEAS Aeronaut J* 2016; 7: 135–148.
4. Oosedo A, Abiko S, Konno A, et al. Development of a quad rotor tail-sitter VTOL UAV without control surfaces and experimental verification. In: *2013 IEEE international conference on robotics and automation*, 2013, pp.317–322. USA: IEEE.
5. Hochstenbach M, Notteboom C, Theys B, et al. Design and control of an unmanned aerial vehicle for autonomous parcel delivery with transition from vertical takeoff to forward flight – VertiKUL, a quadcopter tailsitter. *Int J Micro Air Vehicles* 2015; 7: 395–405.
6. Smeur EJJ, Chu QP, de Croon GCHE, et al. Modelling of a hybrid uav using test flight data. In: de Croon G, van Kampen EJ, De Wagter C, et al. (eds) *International micro air vehicle competition and conference* 2014. Delft, the Netherlands, 2014, pp.196–203. The Netherlands: IMAV.
7. Bataillé B, Moschetta JM, Poinsot D, et al. Development of a VTOL mini UAV for multi-tasking missions. *Aeronaut J* 2009; 113: 87–98.

8. Lustosa L, Defay F and Moschetta J. Development of the flight model of a tilt-body MAV. In: *IMAV*. Delft, the Netherlands, 12-15 August 2014.

9. Bronz M, Smeur E and de Marina H (2017) Development of a fixed-wing mini UAV with transitioning flight capability. In: *35th AIAA Applied Aerodynamics Conference*, Denver, Colorado, 5-9 June 2017.

10. Wong K, Alfredo Guerrero J, Lara D, et al. *Attitude stabilization in hover flight of a mini tail-sitter UAV with variable pitch propeller. In: IEEERSJ international conference on intelligent robots and systems.* San Diego, United States , October 2007.

11. De Wagter C, Ruijsink R, Smeur E, et al. Design, control and visual navigation of the DelftaCopter. *J Field Robot* 2017; 35: 937–960.

12. Kondak K, Bernard M, Losse N, et al. Autonomously flying VTOL-robots: modeling and control. In: *Proceedings 2007 IEEE international conference on robotics and automation,* 2007, pp.736–741. USA: IEEE.

13. De Wagter C and Smeur EJ. Control of a hybrid helicopter with wings. *Int J Micro Air Vehicles* 2017; 9: 209–217.

14. Vorsin D and Arogeti S. Flight transition control of a multipurpose uav. In: *13th IEEE international conference on control automation (ICCA)*, 2017, pp.507–512. Ohrid, Macedonia: IEEE.

15. Roberts J, Frousheger D, Williams B, Campbell D and Walker R. How the Outback Challenge Was Won: The Motivation for the UAV Challenge Outback Rescue, the Competition Mission, and a Summary of the Six Events. I*EEE Robotics & Automation Magazine*, 23(4): 54–62.

16. Gandhi MS, Whitcher L, Theodorou E, et al. Practical system identification for small VTOL unmanned aerial vehicle. In: *AIAA Scitech 2019 forum,* 2019. USA: American Institute of Aeronautics and Astronautics.

17. Bramwell A, Done G and Balmford D. *Bramwell's helicopter dynamics*. USA: American Institute of Aeronautics and Astronautics, 2001.

18. Mettler B. *Identification modeling and characteristics of miniature rotorcraft*. Boston, MA: Springer, 2003, pp.1–24.

19. Mettler B, Dever C and Feron E. Scaling effects and dynamic characteristics of miniature rotorcraft. *J Guid Control Dyn* 2004; 27: 466–478.

20. Kondak K, Bernard M, Losse N, et al. Elaborated modeling and control for autonomous small size helicopters. In: *Proceedings of the ISR/Robotik,* München, Germany, 2006.

21. Bhandari S, Colgren R, Lederbogen P, et al. Six-DoF dynamic modeling and flight testing of a UAV helicopter. In: *AIAA modeling and simulation technologies conference and exhibit*, August, pp.992–1008. San Francisco, California: AIAA.

22. Sandino LA, Bejar M, Ollero A, et al. A survey on methods for elaborated modeling of the mechanics of a small-size helicopter. Analysis and comparison. *J Intell Robot Syst* 2013; 72: 219–238.

23. Tischler MB and Remple RK. *Aircraft and rotorcraft system identification: engineering methods with flight test examples*. AIAA, 2008.

24. Hattenberger G, Bronz M and Gorraz M. Using the Paparazzi UAV system for scientific research. In: *IMAV 2014, international micro air vehicle conference and competition 2014*. Delft, Netherlands, 2014, pp.247–252. Delft, the Netherlands: IMAV.

25. Dorobantu A, Murch A, Mettler B, et al. System identification for small, low-cost, fixed-wing unmanned aircraft. *J Aircr* 2013; 50: 1117–1130.